New Approach Methodology for Assessing Inhalation Risks of a Contact Respiratory Cytotoxicant: Computational Fluid Dynamics-Based Aerosol Dosimetry Modeling for Cross-Species and In Vitro Comparisons

Richard A. Corley,[*,1] Andrew P. Kuprat,[*] Sarah R. Suffield,[*] Senthil Kabilan,[*,2] Paul M. Hinderliter,[†,3] Kevin Yugulis,[‡] and Tharacad S. Ramanarayanan [ID][†,4]

[*]Pacific Northwest National Laboratory, Richland, Washington 99352, USA [†]Syngenta Crop Protection, Greensboro, North Carolina 27409, USA and [‡]Battelle Memorial Institute, Columbus, Ohio 43201, USA

[1]Present address: Greek Creek Toxicokinetics Consulting, LLC, 4659 W. Deer Path Dr., Boise, ID 83714, USA

[2]Present address: Takeda Pharmaceuticals, 40 Landsdowne St., Cambridge, MA 02139, USA

[3]Present address: Alexion Pharmaceuticals, Inc., 121 Seaport Blvd., Boston, MA 02210, USA

[4]To whom correspondence should be addressed at Syngenta Crop Protection, 410 Swing Rd., PO Box 18300, Greensboro, NC 27409, USA. E-mail: tharacad.ramanarayanan@syngenta.com.

ABSTRACT

Regulatory agencies are considering alternative approaches to assessing inhalation toxicity that utilizes *in vitro* studies with human cells and *in silico* modeling *in lieu* of additional animal studies. In support of this goal, computational fluid-particle dynamics models were developed to estimate site-specific deposition of inhaled aerosols containing the fungicide, chlorothalonil, in the rat and human for comparisons to prior rat inhalation studies and new human *in vitro* studies. Under bioassay conditions, the deposition was predicted to be greatest at the front of the rat nose followed by the anterior transitional epithelium and larynx corresponding to regions most sensitive to local contact irritation and cytotoxicity. For humans, simulations of aerosol deposition covering potential occupational or residential exposures (1–50 μm diameter) were conducted using nasal and oral breathing. Aerosols in the 1–5 μm range readily penetrated the deep region of the human lung following both oral and nasal breathing. Under actual use conditions (aerosol formulations >10 μm), the majority of deposited doses were in the upper conducting airways. Beyond the nose or mouth, the greatest deposition in the pharynx, larynx, trachea, and bronchi was predicted for aerosols in the 10–20 μm size range. Only small amounts of aerosols >20 μm penetrated past the pharyngeal region. Using the ICRP clearance model, local retained tissue dose metrics including maximal concentrations and areas under the curve were calculated for each airway region following repeated occupational exposures. These results are directly comparable with benchmark doses from *in vitro* toxicity studies in human cells leading to estimated human equivalent concentrations that reduce the reliance on animals for risk assessments.

Key words: chlorothalonil; CFD; CFPD; aerosol deposition; aerosol clearance; risk assessment.

In response to the National Research Council (NRC) of the National Academies of Science, Engineering and Medicine report on Toxicity Testing in the 21st Century (NRC, 2007), the U.S. Environmental Protection Agency has been evaluating alternative test methods that may reduce the reliance on vertebrate animal testing of chemical substances in the future (EPA, 2016, 2018). More recently, EPA's Office of Pesticide Programs is currently considering new approaches to the assessment of inhalation toxicology using the respiratory irritant, chlorothalonil as a case study (EPA, 2019). In support of this objective, *in silico* models of aerosol dosimetry in the respiratory system described herein were developed to relate results from prior aerosol inhalation studies in rats (Bain, 2013) and new *in vitro* studies with human cells (Vinall, 2017; Li *et al.*, 2018; Hargrove *et al.*, forthcoming) to potential occupational exposures.

Chlorothalonil Toxicity and Modes of Action

Chlorothalonil (2,4,5,6-tetrachloroisophthalonitrile; Supplementary Figure 1) is a broad-spectrum contact (nonsystemic) fungicide that has a history of use on agricultural crops since it was first approved in 1966. Since then, it has been used to control diseases in a variety of fruit, turf, vegetable, and agricultural crops as well as a wood protectant and antimold or antimildew agent (Mozzachio *et al.*, 2008; Wilkinson and Killeen, 1996). Residential uses include golf courses, wood preservatives, and use in paint formulations.

Several reviews on the toxicity, carcinogenicity, and modes of action for chlorothalonil have been published (cf. IARC, 1999; Mozzachio *et al.*, 2008; Wilkinson and Killeen, 1996). In brief, chlorothalonil has been shown to be a direct-acting irritant/cytotoxicant in the portal of entry tissues following all routes of exposure. Following repeated or prolonged exposures, irritation, inflammation (with accompanied inflammatory cell infiltration), and necrosis or ulceration of epithelial tissues followed by cell proliferation and tissue remodeling have been observed in skin, forestomach, and respiratory tissues of laboratory animals.

Because chlorothalonil is essentially a nonvolatile, white, crystalline solid that is practically insoluble in water and only slightly soluble in organic solvents (IARC, 1999), chlorothalonil is formulated in either liquid or solid forms that are ultimately diluted before application. Potential human exposures are thus associated with the mixing process, dilute aerosol formulations from spray applications or deposited residues.

As part of the pesticide re-registration process, EPA historically required registrants and manufacturers to conduct subchronic inhalation studies in laboratory animals to evaluate the potential health effects of pesticides in residential or occupational settings. In advance of conducting subchronic inhalation studies for re-registration, a 2-week aerosol inhalation range-finding toxicity study was conducted in male Sprague Dawley rats with the commercial formulation, Bravo Weather Stik 720 SC at targeted concentrations ranging from 0.001 to 0.015 mg chlorothalonil/l of air (Bain, 2013; Supplementary Table 1). During the course of the 2-week study, toxicologically significant observations related to respiration (wheezing, sneezing, irregular respiration, gasping) were initially observed in 2 out of 25 animals in the high exposure group but resolved over the second week of treatment. A concentration-dependent reduction in feed consumption and body weight gains was also observed, with net weight loss occurring in the highest exposure group.

As anticipated from prior acute inhalation studies and longer-term studies by other routes of exposure, the primary pathological findings included concentration-dependent epithelial cell degeneration and necrosis with associated inflammation and inflammatory cell infiltration, hyperplasia and squamous metaplasia in respiratory tissues lining the nasal cavity, larynx, trachea, and lung of male Sprague Dawley rats (see Supplementary Table 2). All microscopic findings in respiratory tissues were indicative of a contact irritant/cytotoxicant that showed partial (nose and larynx) or full (trachea and lungs) recovery at the end of a 14-day post-exposure recovery period depending upon the exposure concentration. A no-observed adverse effect level (NOAEL) was not established under these exposure conditions with nasal respiratory epithelium and larynx being particularly susceptible tissues.

New Approach Methodologies for Assessing Chlorothalonil Inhalation Risks

The value of conducting longer-term inhalation rodent bioassays becomes questionable for chemicals like chlorothalonil, where the local portal of entry contact cytotoxicity is the most sensitive endpoint that limits exposure concentrations and durations. This is especially applicable for a species that, unlike humans, are obligate nose breathers with significantly different nasal and laryngeal airway anatomy leading to potentially important differences from humans in target tissue doses.

Therefore, *in lieu* of conducting additional longer-term inhalation studies in rats, a series of *in vitro* studies with commercially available primary human respiratory epithelial cells grown at a 3D air-liquid interface (ALI) were conducted to directly assess the local dose-response relationships for cytotoxicity (Vinall, 2017). To integrate these new studies for inhalation risk assessments, computational aerosol dosimetry models are needed to relate realistic human exposure scenarios to the dose-response relationships determined *in vitro* and from *in vivo* animal studies.

Several options are available to estimate respiratory tissue dosimetry following inhalation exposures to aerosols, each with its strengths and weakness. Two such models have been used by the EPA to estimate aerosol deposition in the respiratory tracts of laboratory animals and humans—the regional deposited dose (RDD) model and the multiple path particle dosimetry (MPPD) model (Kuempel *et al.*, 2015). MPPD in particular is widely used and readily available (https://www.ara.com/products/multiple-path-particle-dosimetry-model-mppd-v-304) with both models serving as reasonable screening and cross-species comparative tools if toxicity is associated with total or regional deposition. However, the toxicity of many inhaled agents to respiratory tissues, such as those observed for chlorothalonil, are often site-specific and highly dependent upon each species unique anatomy and physiology, not just the agent and exposure conditions (Kimbell *et al.*, 2001; Corley *et al.*, 2012, 2015; Kabilan *et al.*, 2016).

The present study was therefore conducted to quantitatively compare site-specific aerosol deposition patterns and local surface doses of chlorothalonil within regions of the conducting airways of the rat and human using anatomically and physiologically correct, 3D computational fluid dynamics (CFD) airflow and Lagrangian aerosol transport models (also known as computational fluid-particle dynamics or CFPD models). Simulations were conducted under previously reported inhalation bioassay conditions for rats as well as across a broad range of aerosol sizes that encompass the sizes expected for occupational and residential exposure for humans to facilitate cross-species and *in vitro* to *in vivo* comparisons of exposure—localized respiratory tissue dose-response relationships. The

resulting computational models provide the necessary common denominator of localized tissue doses critical to integrating data and defining appropriate comparative dose-metrics within a source-to-outcome risk assessment approach.

MATERIALS AND METHODS

Rat and human model structures. Both the rat and human airway models used in the present study were adapted from previously published CFD models (Corley et al., 2012, 2015; Kabilan et al., 2016). The rat airway geometry was based upon micro-CT imaging of the upper airways of a male Sprague Dawley rat weighing 309 g at an isotropic resolution of 50 μm using a GE eXplore CT120 scanner. The rat model was limited to upper airways from the nares through the upper trachea to reduce computational requirements and focus simulations on the most sensitive target tissues (respiratory and transitional epithelium in the nose and larynx).

Two human models, 1 for nasal and 1 for oral breathing, were derived from multislice CT imaging of a 35-year-old healthy male volunteer, weighing 68 kg and 67 inches tall. A GE Light Speed Discovery CT750 was used to produce a volumetric image sequence with a resolution of $0.7 \times 0.7 \times 0.5$ mm in the x, y, and z dimensions. Segmentation and widening of the larynx from the "as-imaged" supine breath-hold position to a fully open geometry that occurs during inhalation in an upright posture was performed as described in Kabilan et al. (2016). Additional segmentation of the oral cavity through the epiglottis was conducted using Materialise Mimics (Innovation Suite 22.0) with cleaning and modifications (repositioning surface of the tongue for upright oral breathing and closing off the connection to the esophagus) using Materialise 3-matic (Materialise, Plymouth, Michigan). For the current study, human simulations were designed for nasal and oral breathing typical for resting or light activity although the model may be reconfigured for multiple breathing patterns in the future. The resulting male human nasal breathing model extended from the nares to the trachea to encompass the most sensitive target tissues observed in the rat, the types of epithelial cells used in ALI tissue culture models, and expected deposition from occupational exposures to chlorothalonil-containing aerosols. The oral breathing model extended from the mouth to the tracheobronchial region within the resolution of the CT images (typically 5–10 generations) to capture additional aerosols not otherwise filtered by nasal airways.

Computational mesh development and evaluation for aerosol dosimetry. All airway surfaces extracted from the rat and human CT imaging data were assigned cell type (nose) or regional designations (mouth, pharynx, larynx, trachea, carina, bronchi) as described previously (Corley et al., 2015; Kabilan et al., 2016) to facilitate reporting of aerosol deposition results for cross-species, breathing modality, and *in vitro* comparisons. Hybrid prism/polyhedral volume meshes were generated in STAR-CCM+ (Version 8.02 for the nasal breathing model developed at PNNL and version 14.04.011 for the oral breathing model developed later at Battelle Memorial Institute, Siemens PLM, Plano, Texas). The tightly packed boundary layer consisted of prismatic elements to accurately capture boundary layer airflows and deposition of aerosol droplets at the airway walls. Polyhedral mesh elements constituted the core of the volume meshes (Figure 1). Mesh independence studies were conducted to assess the sensitivity of predicted aerosol deposition to element size and transitions between polyhedral and prism elements for both species.

For the rat, the width of the prismatic boundary layer was kept constant at 80 μm, whereas the number of layers was increased (5, 10, 15, and 20 layers corresponding to 1.42, 4.28, 9.72, and 18.7 million elements, respectively). The largest mesh represented an upper limit for computational efficiency and facile visualization for transient aerosol simulations using a mid-level parallel computer (~100–200 hundred processors) common to most computing facilities. Simulations were initially conducted using exposure conditions from the 2-week inhalation study (2.72 μm mass median aerosol diameter [MMAD], 4.03 mg total aerosol/l of air; Supplementary Table 1). To reduce the overall computational costs, Star CCM+ tracks parcels, where the number of aerosol particles in each parcel is equal to the total particle flow rate at each inlet location (based upon air concentration, local airflow, and particle characteristics) multiplied by time-step size, divided by the total number of seed points for parcel introduction to flow streams. Convergence was achieved in all but the laryngeal compartment (which represented <0.5% of inhaled aerosol deposition) in the 9.72 million-element mesh; therefore, the largest, 18.7 million-element mesh was used for final simulations.

For the human nasal model, the width of the prismatic boundary layer was kept constant at 0.5 mm, whereas the number of layers and total elements was increased (10, 20, and 30 layers corresponding to 1.37, 2.85, and 5.10 million elements, respectively). A uniform grid of X-Y coordinates for aerosol seed points was used to facilitate comparisons across multiple aerosol sizes. Simulations were performed at 1, 10, and 30 μm aerosol size for each mesh under otherwise identical aerosol exposure conditions. The convergence of predicted regional aerosol deposition for each aerosol size was achieved with the medium-sized mesh (20 prismatic boundary layers and 2.85 million elements overall; Figure 1B); this mesh was used for the remaining human nasal simulations. The oral breathing model was adapted from the final nasal model and contained 4.88 million elements with 15 prismatic boundary layers (Figure 1C). Characteristics of the final meshes used for both the rat and human CFD models and aerosol simulations are summarized in Table 1.

Airflow simulations. CFD airflow simulations were performed using STAR-CCM+. Airflow predictions were based upon the turbulent 3D, incompressible mass, and Reynolds-averaged Navier-Stokes momentum equations. The generation and dissipation of turbulence were accounted for using the SST k-omega model with $y+ < 1$ to resolve laminar sublayer flows near the walls. This model has been shown previously to perform well for swirling flows such as those produced under transient airflow conditions in nasal tissues and the larynx (Corley et al., 2015; Kabilan et al., 2016). The model was formulated by blending the standard k-omega model near the surface with a transformed k-epsilon model in the bulk flow.

For all CFD simulations, air at room temperature was considered the working fluid, with a density of 1.204 kg/m^3 and a dynamic viscosity of 1.8×10^{-5} Pa-s corresponding to properties of air at 20°C. The inlets for both species were prescribed a time-dependent flow rate boundary condition where the CFD code adjusted the magnitude of the inlet velocity to match the user-specified volumetric flow rate and breathing profile. A transient inhalation profile corresponding to a minute volume of 0.217 liters with a breathing frequency of 100 breaths per minute was used to drive the simulations for the rat and a minute volume
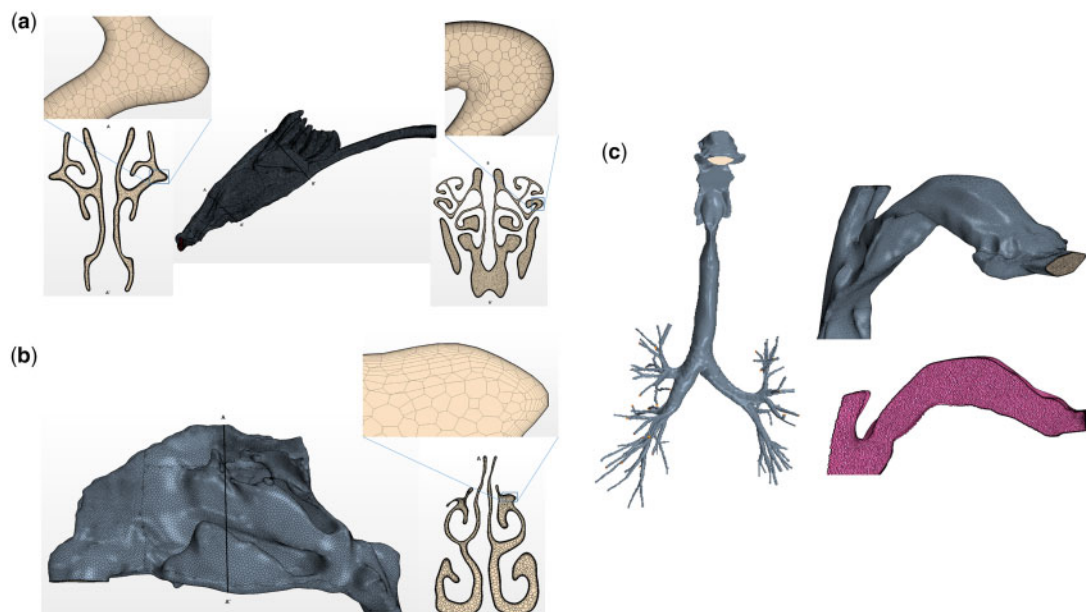
Figure 1. Hybrid polyhedral meshes generated in STAR-CCM+ for the (A) rat nose, (B) human nose, and (C) human mouth with selected cross-sectional planes showing close-ups of the polyhedral core and prismatic boundary layers.

Table 1. Computational Mesh Characteristics and Particles Tracked for the Rat and Human CFD Models

Characteristic	Rat	Human (Nasal)	Human (Oral)
General mesh statistics			
Surface facets	857,261	132,265	345,781
Prism boundary layers	20	20	15
Cells in boundary layer	17,145,220 (est.)	2,645,300 (est.)	4,250,764
Boundary layer thickness (μm)	80	500	500
Total polyhedral and prismatic cells in mesh	18,699,463	2,845,876	4,880,020
Nodes	45,127,197	6,433,388	12,022,936
Maximum Y+ value (dimensionless)	0.238 (dry squamous)	0.122 (vestibule)	0.09 (bronchi)
Meshing/simulation software (Star-CCM+) version	8.02	8.02	14.04.011
Boundary inlet			
Surface facets	6,300	3,690	9,620
	(5 triangular, 4780 quadrilateral, 1515 polygonal)	(3151 quadrilateral, 539 polygonal)	(4650 quadrilateral, 4970 polygonal)
Surface area (m^2)	3.92297×10^{-6}	1.51431×10^{-4}	1.42×10^{-4}
Representative no. parcels[a] tracked/simulation	2.14×10^6	4.0×10^5	9.91×10^6

[a]To reduce the overall computational costs, Star CCM+ tracks parcels, where the number of particles in each parcel is equal to the total particle flow rate (based upon air concentration, airflow, and particle characteristics) divided by the total number of injection points (the particles are distributed evenly over the number of injectors). One parcel was introduced at each injection point (based upon X-Y grid coordinates within the airway lumen at each time step in the simulation)..

of 7.4 liters and breathing frequency of 20 breaths per minute for the human nasal and oral breathing models (ICRP, 1994). A simple sine wave based upon the respective minute volumes and breathing frequencies was used to drive the simulations for each species and breathing modality. A zero-pressure boundary condition was used at the outlets (trachea or bronchi) and a no-slip wall condition was applied at remaining airway boundaries, which were assumed to be rigid and impermeable.

Aerosol simulations. The standard Lagrangian particle tracking algorithm in STAR-CCM+ was utilized in the CFPD model with the following assumptions: (1) 1-way coupling of airflow with aerosol transport (eg aerosol droplets do not affect airflows; an assumption that could become less valid for simulating aerosols

larger than the ones used for the rat given their small nasal airways); (2) no aerosol agglomeration, hygroscopic growth, or electrostatic interactions; (3) aerosol droplet diameter was assumed to be constant for each simulation; (4) aerosol density was based upon water (1 g/cm^3), the diluent used in inhalation studies and application methods; (5) all aerosols were introduced in specified X-Y coordinates within the nasal or oral inlets based upon localized airflow and aerosol exposure concentrations at each time-step and thus, considered fully inhalable at all sizes; (6) no-slip boundary condition was used for aerosols at the airway wall; (7) once the aerosol collides with the wall it was considered "stuck" at the point of impact and does not slide along the wall or re-enter the airflow; (8) the only forces assumed to act on the aerosols were drag and gravity

with the gravity force directed for a prone rat and upright human; (9) mechanisms for aerosol deposition appropriate for the physical characteristics of the simulated aerosols included sedimentation, inertial impaction, and diffusion although the latter mechanisms is more important for smaller ($<1\,\mu$m) aerosols; and (10) airways were assumed smooth and rigid as is the current standard for CFD simulations of the upper respiratory tract.

All CFPD calculations of aerosol droplet deposition across species and aerosol sizes represent initial deposition patterns during a single inspiratory breath. Without a complete distal lung model capable of simulating the aerosol transport and deposition into and out of the deep lung, simulations were restricted to the initial inhalation phase of the normal breathing cycle. Calculations of deposited aerosol doses in each region of the airways (mg aerosol/cm^2 of epithelial surface deposited) were calculated for each surface element in each simulation as well as mass-balance determinations of aerosols deposited, suspended in airway lumens at end of inhalation, and escaping the trachea (nasal breathing rat and human models) or bronchi (human oral breathing model) for each simulation. Calculations of chlorothalonil deposited airway doses (mg chlorothalonil/cm^2 of epithelial surface deposited) were then calculated based upon water dilutions of Bravo Weather Stik 720 SC. For example, a typical water dilution in-ground spray tanks for agricultural spray operations is 4.9% chlorothalonil w/w (Flack *et al.*, 2019). Recalculations of deposited tissue doses of the active ingredient can be readily performed using the reported aerosol deposited dose (mg aerosol/cm^2) and user-defined percentages of chlorothalonil in the aerosol. Likewise, deposition profiles from alternative exposure concentrations and polydisperse aerosol size distributions can be calculated from the existing monodisperse simulations given the assumptions of no aerosol-aerosol or aerosol-airflow interactions for each aerosol size.

Aerosol clearance model for repeated human exposures. The current CFPD model is restricted to the upper conducting airways (nose through trachea or bronchi) where mucociliary clearance is rapid relative to the deep lung leading to a large fraction of deposited aerosols being cleared from this region within 24 h (Asgharian *et al.*, 2001). As a result, the conversion of local tissue doses of aerosols containing chlorothalonil following a single inhaled breath to multiple breaths or repeated exposure scenarios requires a model of clearance before CFPD results can effectively be used for calculations of human equivalent exposure concentrations (HECs) associated with *in vivo* animal studies in traditional risk assessments or *in vitro* studies with human cells such as those proposed as an alternative point of departure (POD) for chlorothalonil (Vinall, 2017; Li *et al.*, 2018; Hargrove *et al.*, forthcoming).

Of the numerous clearance models that have been developed from experimental data in animals and humans (cf. Lippman *et al.*, 1980; Lippman and Schlesinger, 1984; Stuart, 1984; Asgharian *et al.*, 2001; ICRP, 1994; Paquet *et al.*, 2015), the recent Paquet *et al.* (2015) model was selected to simulate repeated exposures to aerosols for the current study. This model was chosen because of its expansive data and validation process for its use in assessing risks of occupational exposures to radionuclides, and for a structure that maps reasonably well to the upper airways in the current human CFPD models.

Simulations of retained local doses for each aerosol size in the human were therefore developed using CFPD model predictions of local deposited dose (total aerosol deposited normalized to deposited surface area) for a single inhaled breath as inputs to the anterior nose (vestibule; ET1), posterior nose (respiratory, olfactory, pharynx, larynx; ET2), and tracheobronchial (BB) regions of the clearance model (Figure 2). The current model was coded using Magnolia (ver 1.3.9Beta; available at https://www.magnoliasci.com) as shown in the Supplemental Material. Repeated exposures with the clearance model were performed assuming the same ventilation profile at 20 bpm used in the CFPD model to define deposition, retention, and clearance for a standard workweek (5 consecutive days of 8-h exposures/day followed by 2 days of no exposure). Maximum concentrations (C_{max}) and areas under the curve (AUCs) for retained local doses in each region were determined for the final day of exposure using Microsoft ExcelÒ with add-in PK functions developed by Usansky *et al.* at Allergan (Irvine, California).

Approvals. All CFPD models were developed from prior published studies that were conducted according to all local and international ethics standards for animal and human research. The Institutional Animal Care and Use Committees of PNNL and the Institutional Review Boards of the University of Washington and PNNL approved all animal studies and human volunteer work conducted under a separate grant that provided the airway imaging data for this project.

RESULTS

Rat Simulations

For the rat, simulations were conducted using the overall average aerosol concentration (4.03 mg/l) and size (2.72 μm) from the 2-week inhalation toxicity study with water dilutions of the Bravo Weather Stik 720 SC formulation containing 53.7% (w/w) chlorothalonil (Bain, 2013; Supplementary Table 1). Regional deposition efficiencies (% of inhaled aerosol) and deposited doses (mg aerosol/cm^2 deposited surface areas) are summarized in Table 2. Under this exposure condition, the greatest percentage of inhaled 2.72 μm aerosol droplets deposited in the anterior, ventral portion of the nose (53.1% in the dry squamous epithelium of the nostril, 4.83% in the wet squamous) with all remaining upper airway tissue compartments receiving significantly less than 1% of the total inhaled dose.

The deposition of chlorothalonil-containing aerosols occurred in highly discrete areas within each region of the rat respiratory airways with only 1.2% of the total surface area receiving any predicted deposition (Table 2 and Figure 3A). Even within these discrete regions of deposition, the deposited aerosol doses (mg aerosol/cm^2 deposited surface area) varied widely. For example, the aerosol masses deposited in each individual surface facet (mg aerosol deposited/cm^2 of deposited surface facet) of each tissue compartment were rank ordered as a function of the surface facet's fraction of the deposited surface area for each tissue type (see Supplementary Figure 2 for representative plots of the dry squamous and respiratory epithelial compartments of the nose and the larynx of the rat). Within each region, the distribution of deposited doses in each surface facet deviated considerably from the simplified assumption that total deposited mass is distributed evenly within a compartment. As a result, descriptive statistics (range and percentiles of deposited doses in surface elements) are reported for each tissue type along with the surface areas with deposition (Supplementary Tables 3 and 4).

Conceptually, the determination of local "hot spots" for comparison of airway surfaces with the greatest deposition across species or with *in vitro* studies is similar to, but not as straight forward as, the approach used in prior CFD/PBPK models for
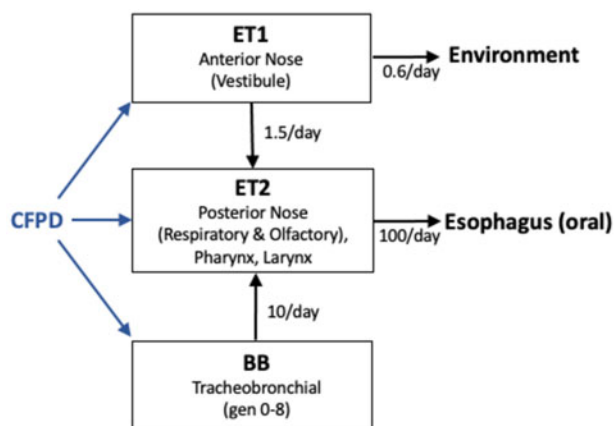
Figure 2. Diagram of clearance model for the extrathoracic (ET1, anterior nasal tissues; ET2, posterior nasal, pharynx, larynx) and tracheobronchial (BB trachea, bronchial generations 0–8) regions covering CFPD simulations based upon Paquet *et al.* (2015). Rate constants for clearance between compartments and to the environment or esophagus (oral consumption) are shown. Simulations were initiated by CFPD-deposited dose for each region as described in the text and Supplementary Material.

reactive gases or vapors (Corley *et al.*, 2015). In this case, the fraction of surface areas with any aerosol deposition can be small (eg, 1.2% of total surface area for the rat CFPD model) and variable, depending upon aerosol size, concentration, and breathing dynamics. Deposited masses can also vary significantly across deposited surface elements that may not be contiguous within a region with large areas of no deposition, unlike the case with gases and vapors. Thus, for this study, the total mass over the total deposited surface for each tissue compartment was evaluated as a potential dose metric for cross-species and *in vivo* to *in vitro* comparisons. Other dose metrics could be considered but as discussed below, but final choice should ultimately be correlated with site-specific tissue responses.

For the rat, the regional doses of chlorothalonil at the lowest adverse effect level (LOAEL) from the 2-week inhalation study were calculated from the analytical determinations of chlorothalonil exposure concentrations (Supplementary Table 1) and the deposited aerosol doses (Table 2) in each region of the airway model. The distributions of chlorothalonil deposited doses (mg chlorothalonil/cm^2) were thus directly proportional to the overall aerosol mass deposition based upon concentrations of the active ingredient in each aerosol exposure following a single inhaled breath (Supplementary Table 5). Consistent with the most sensitive tissues for local irritation/cytotoxicity (Supplementary Table 2), the greatest local deposited doses of chlorothalonil were achieved in the larynx followed by the anterior transitional epithelium for aerosols that penetrated past the dry and wet squamous epithelium at the front of the nose assuming a monodisperse, 2.72-μm aerosol exposure.

Human Nasal Breathing Simulations

Human nasal breathing simulations were also conducted using the same exposure and aerosol characteristics from the 2-week rat inhalation study. Compared with the rat simulations, where over 58% of inhaled 2.72 μm-sized aerosols were retained in the nose, primarily in the anterior dry and wet squamous epithelial regions, >99% of inhaled 2.72 μm aerosols penetrated past the human nose (Figure 3B).

To characterize potential local and regional dosimetry of chlorothalonil in the upper conducting airways of humans (nose through the trachea) following inhalation exposures under potential use conditions, aerosol sizes ranging from 1 to 30 μm MMAD were simulated at a representative air concentration of 1 mg/l. This range of aerosol sizes was chosen to cover expected sizes in residential or occupational exposures and to facilitate calculations of polydisperse aerosol deposition in future risk assessments (Flack *et al.*, 2019). This exposure concentration also simplifies extrapolation to other water dilutions of the active ingredient but on its own should be considered a very high exposure for formulations that are unlikely to be tolerated by humans exposed to contact respiratory irritants like chlorothalonil. For future extrapolations to significantly less than 1 mg/l aerosol exposure concentrations, CFPD simulations should be repeated to confirm local dose

Table 2. Aerosol Deposition and Deposited Doses of Chlorothalonil (CTN) in Each Region of the Rat Model Following a Single Inhaled Breath at the LOAEL of 0.0011 mg CTN/l

| Airway Region | Surface Area (cm^2) | Regional Aerosol Deposition (4.03 mg/l, 2.72 μm MMAD) | | | | | Regional CTN Dose at LOAEL (0.0011 mg/l) | |
		Total Deposition (% Inhaled)	Surface Area Deposited (cm^2)	Fraction Regional Surface Area Deposited	Total Aerosol Deposited in Region (mg)	Total Aerosol in Deposited SA (mg/cm^2)	Total CTN Deposited (mg)	Total CTN in Deposited SA (mg/cm^2)
Vestibule, dry squamous	0.45	53.10	0.077	0.170	2.97E-03	3.87E-02	8.56E-07	1.11E-05
Wet squamous	0.63	4.83	0.054	0.087	4.06E-04	7.49E-03	1.17E-07	2.16E-06
Respiratory	5.69	0.10	0.051	0.009	8.26E-06	1.61E-04	2.38E-09	4.65E-08
Transitional	2.16	0.16	0.011	0.005	1.35E-05	1.26E-03	3.90E-09	3.63E-07
Olfactory	6.75	0.02	0.013	0.002	1.70E-06	1.35E-04	4.89E-10	3.90E-08
Pharynx	1.32	0.02	0.021	0.015	1.60E-06	7.81E-05	4.61E-10	2.25E-08
Larynx	0.38	0.32	0.018	0.047	2.68E-05	1.50E-03	7.72E-09	4.31E-07
Trachea	2.48	0.002	0.002	0.001	1.74E-07	7.51E-05	5.02E-11	2.16E-08
Total	19.87	58.55	0.246	0.012	3.43E-03	1.39E-02	9.88E-07	4.01E-06

Simulations conducted for 4.03 mg/l aerosol concentrations with a mass median aerosol diameter (MMAD) of 2.72 μm used in the 2-week inhalation study of Bain (2013). Ranges and percentiles for aerosol deposition and regional chlorothalonil doses in each compartment are summarized in Supplementary Tables 3–5. Simulation results were truncated to a level of precision for calculation and display purposes and not to imply the level of certainty to the results.
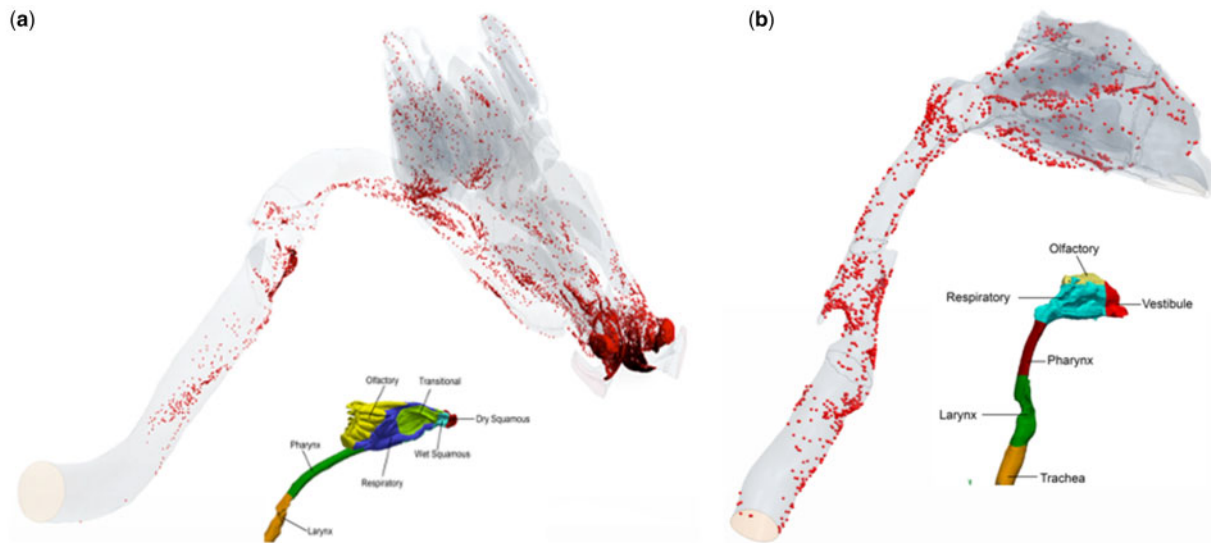
Figure 3. Deposition patterns in the (A) rat and (B) human nasal breathing models exposed to 2.72 μm MMAD aerosols at a concentration of 4.03 mg/l used in the 2-week inhalation study in rats (Bain, 2013). Annotated surfaces of the rat and human airway models showing positions of cell type (nose) and regions (pharynx, larynx, trachea) used to report regional aerosol deposition are shown in respective inserts.
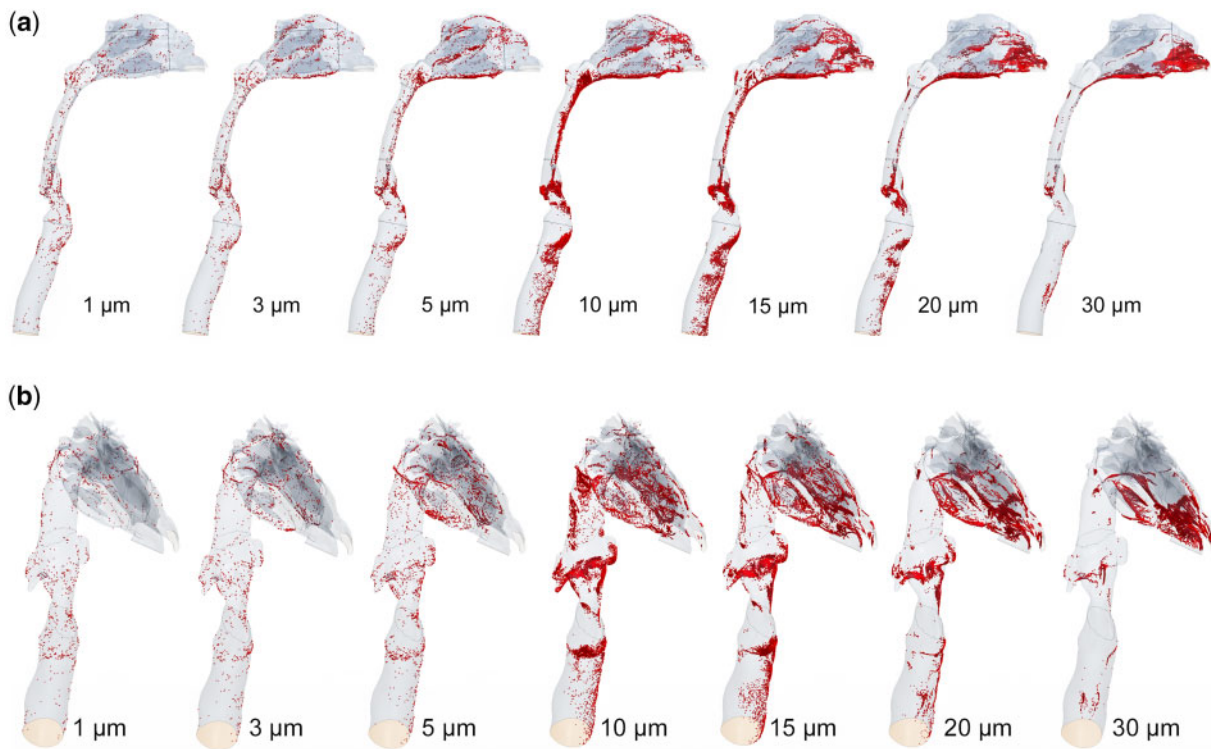

Figure 4. Deposition patterns in the human nasal model following exposures to 1 mg/l aerosols with 1, 3, 5, 10, 15, 20, and 30 μm MMAD aerosols. Top-side view; bottom-ventral view.

predictions because deposited surface areas may decrease. As with the rat, all simulations were conducted for a single, inhaled breath associated with resting or light activities with aerosol droplets that leave the trachea not available for the return during exhalation.

For 1 and 3 μm aerosol sizes, very little deposition occurs in the upper conducting airways (<1% of total inhaled) with most of the inhaled aerosols (nearly 80% inhaled) exiting the trachea and thus available for penetration to the lung where they can

either deposit or return during exhalation (Figure 4 and Table 3). The remaining mass (~20% inhaled) was suspended in the airway lumen and available for deposition or exhalation during the exhalation phase of the breathing cycle. As aerosols increase in size, the shift towards upper airway deposition significantly increases to 2.35%, 48.77%, 86.91%, 95.05%, and 98.85% inhaled at 5, 10, 15, 20, and 30 μm MMAD, respectively (Table 4) with corresponding decreases in the amounts suspended in the airway lumen or exiting the trachea at the end of the inhalation

Table 3. Mass Balance of Inhaled Aerosols That Either Deposit on Airway Surface, Leave the Trachea Outlet, or Remain Suspended in the Airway Lumen at the End of the Inhalation Phase of a Single **Human** Breath Exposure to 1 mg/l Aerosol Over Sizes Ranging From 1 to 50 μm MMAD

Aerosol Size (μm)	Human Nasal (Nose through trachea)			Human Oral (Mouth through bronchi)		
	Total Deposition (% Inhaled)	Suspended in Airway Lumen (% Inhaled)	Total Exiting Trachea Outlet (% Inhaled)	Total Deposition (% Inhaled)	Suspended in Airway Lumen (% Inhaled)	Total Exiting Bronchi Outlets (% Inhaled)
1	0.56	20.4	79.0	1.3	33.2	65.5
3	0.72	20.8	78.5	2.0	32.9	65.1
5	2.35	20.9	76.8	4.7	32.6	62.8
10	48.8	17.2	34.1	31.0	30.3	38.6
15	86.9	8.1	5.0	69.1	21.8	9.1
20	95.1	3.8	1.2	87.8	11.6	0.6
30	98.9	1.1	0.03	96.8	3.2	0.0
50	—	—	—	99.5	0.5	0.0

Simulation results were truncated to a level of precision for calculation and display purposes and not to imply the level of certainty to the results.

phase of the breathing cycle (Table 3). For this human CFPD model and exposure conditions, relatively little deep lung penetration is likely to occur for aerosol >10 μm in size based upon corresponding simulations with the MPPD model.

At the larger aerosol droplet sizes, very little penetration past the nasal vestibule is predicted with greater influence of gravity compared with the impaction shift deposition from the walls and upper regions of the nose, including the olfactory epithelium, towards the floor of the nose (Figure 4 and Table 4). Peak deposition and surface areas exposed for respiratory epithelium in the nose, the pharynx, larynx, and trachea occurred with 10–15 μm-sized aerosols (Figure 5). Larger aerosols were increasingly filtered by the nasal vestibule thereby reducing the amounts that penetrated into the conducting airways. Even so, the surface areas of each region where deposition occurred were <20% for any aerosol size at a 1 mg/l exposure concentration. Beyond the nasal vestibule, peak regional doses (mg aerosol/cm^2 deposited surface) occurred for 10–20 μm-sized aerosols with the nasal respiratory, pharynx, and larynx regions receiving the highest doses, similar to regions receiving the highest deposition in the rat.

Site-specific deposited mass (mg deposited/cm^2 deposited surface area) also varied significantly within each tissue region with the data presented as ranges and percentiles (Supplementary Table 6). As with the rat, a small fraction of airway surfaces with deposited aerosols had significantly greater deposited mass than the overall deposited tissue dose/deposited surface area averages calculated for each region while the major fraction of the deposited surface areas has significantly less exposure than average. To illustrate, the rank ordering of human airway surface facets with the deposited mass in nasal respiratory epithelium and larynx following a representative 10 μm-sized aerosol exposure is plotted as a fraction of each compartment's deposited surface areas in Supplementary Figure 3. A vast majority of surface areas for most tissues beyond the vestibule received no deposition whatsoever, regardless of aerosol size (Figure 5B).

Human Oral Breathing Simulations

Simulations of aerosol deposition during oral breathing were also conducted using the same exposure conditions and light-activity breathing profile used in the nasal breathing simulations. Because less deposition occurred in the mouth versus the nose, the oral breathing model was extended from the trachea into the bronchiolar region up to the limits of reliable segmentation from the available CT data from this volunteer to capture a larger fraction of aerosols that exit the trachea. One additional aerosol size, 50μm, was also included to define the upper bounds on total deposition within the available CFD domain.

Even with the more extensive lung model for oral versus nasal breathing, over 60% of inhaled particles exited the bronchial airway outlets for aerosol sizes of 1–5 μm MMAD and were thus available to penetrate into the deeper lung (Table 3). However, just as with the nasal breathing simulations, significantly greater aerosol deposition occurred as aerosol sizes increased from 10 to 50 μm with deposition progressively shifting toward the upper airways and mouth (Table 5). The sites of deposition of the aerosols in the oral breathing model are shown in Figure 6.

As with the nasal model, peak regional deposition (% inhaled) past the mouth (or nose) occurred with 10–15 μm aerosols (larynx, trachea, carina, and bronchi) or 20 μm aerosols (pharynx) (Figure 7). Once particles reach the oropharyngeal region in both models, the general sites of deposition were consistent between the two breathing modalities. Again, without aerosol scrubbing within the nasal region, greater masses of aerosols, especially 10 μm or greater in size, following oral breathing reach the pharynx and beyond which in turn deposit over a larger surface area than observed in the prior nasal breathing model. This larger surface area exposed spreads out the greater aerosol mass for particles pharynx, larynx, and trachea resulting in fairly comparable doses in terms of mg deposited/cm^2 deposited surface area between the 2 models (Figs. 5C and 7C).

Calculations of Retained Doses in Humans for Repeated Exposures

CFPD model predictions from both the prior nasal and oral models provide site-specific estimates of deposited aerosol dose following a single inhaled breath. To use such information in potential risk assessments, deposited dose estimates cannot simply be multiplied by the number of breaths and exposure duration without accounting for clearance processes. Otherwise, the cumulative deposited doses climb linearly (and unrealistically) with each subsequent breath. To determine retained local doses of deposited aerosols for repeated exposures, the single breath outputs from the nasal and oral breathing CFPD models were used as inputs into the Paquet et al. (2015) human particle clearance model (Figure 2,

Table 4. Aerosol Deposition (% Inhaled and Total Deposited Dose Over Deposited Surface Area) for Each Annotated Region of the **Human Nasal Breathing Model** Following Single Breath Exposure to 1 mg/l Aerosol at Sizes Ranging From 1 to 30 µm MMAD

Aerosol Diameter (µm)	Total Deposition (% Inhaled)	Regional Aerosol Deposition (% Inhaled)						Regional Aerosol Deposition (Total mg/cm² Deposited Surface Area)					
		Vestibule	Respiratory	Olfactory	Pharynx	Larynx	Trachea	Vesti-bule	Respiratory	Olfactory	Pharynx	Larynx	Trachea
1	0.56	0.01	0.31	0.003	0.04	0.14	0.05	7.73E-04	6.33E-04	9.12E-04	3.27E-04	4.01E-04	1.38E-04
3	0.72	0.04	0.37	0.037	0.05	0.17	0.06	7.08E-04	3.73E-04	7.72E-04	2.52E-04	4.65E-04	1.45E-04
5	2.35	0.69	1.05	0.176	0.07	0.28	0.09	5.35E-03	4.78E-04	1.76E-03	2.37E-04	5.66E-04	1.27E-04
10	48.8	27.1	12.7	0.024	1.92	5.99	0.99	4.83E-02	3.18E-03	2.82E-04	1.57E-03	3.47E-03	4.49E-04
15	86.9	68.7	9.82	0.009	1.44	3.61	3.48	6.44E-02	2.61E-03	1.23E-04	2.51E-03	2.20E-03	1.31E-03
20	95.1	86.0	7.16	0.001	0.64	0.75	0.52	6.49E-02	2.21E-03	1.18E-04	3.61E-03	6.92E-04	3.74E-04
30	98.9	97.0	1.70	0	0.03	0.09	0.02	6.33E-02	6.57E-04	0	1.94E-04	2.68E-04	5.18E-05

Additional aerosol deposition totals, surface areas deposited, and percentiles are shown in Supplementary Table 6. Simulation results were truncated to a level of precision for calculation and display purposes and not to imply the level of certainty to the results.

Supplementary Material) to perform a repeated exposure scenario for a representative work week (8 h/day for 5 consecutive days followed by 2 days of no exposure).

Figure 8 shows a representation of the impact of physical clearance mechanisms (ie, mucociliary clearance) for a 10 µm-sized aerosol in nasal respiratory (ET1), larynx (ET2), and tracheal (BB) regions from the nasal model. As demonstrated in each region, cumulative deposition increases linearly with each breath until exposures cease while retained doses peak and clear in each region each day due to the relatively high clearance rates in upper conducting airways. Overall, most of the deposited dose was cleared to the esophagus for potential oral uptake with the remainder cleared to the environment or retained in the respiratory tract until completely cleared after exposures ceased. In this example, retained doses in each region reached a day-to-day steady state within 2–3 days of 8-h/day inhalation exposure with most of the retained dose being cleared from each compartment within 24 h after exposures ceased consistent with expectations from the full Paquet et al. (2015) and other prior clearance models (Asgharian et al., 2001).

The profiles for retained airway surface doses over time in these conducting airways (Figure 8) are similar to those encountered in tissue or blood profiles in standard pharmacokinetic studies with soluble drugs or chemicals following inhalation (or other) routes of exposure. Thus, for a contact irritant/cytotoxicant like chlorothalonil, standard pharmacokinetic parameters like peak dose (C_{max}, mg/cm² deposited surface) or AUC (mg*min/cm² deposited surface) can provide important dose metrics for comparisons across species or to in vitro studies or can be used as the basis for determining human equivalent exposures in potential risk assessments.

As an example of this process, C_{max} and AUC values for retained regional aerosol doses for each aerosol size from both the nasal and oral models were converted to corresponding chlorothalonil doses assuming human exposures were to the LOAEL concentration of 0.0011 mg/l from the 2-week inhalation toxicity study in rats (Bain, 2013). For comparison, the in vitro benchmark dose (BMD) (lower 95% confidence limit or BMDL) for cytotoxicity derived from exposure of human respiratory cells from 5 donors grown at the ALI (Vinall, 2017; Li et al., 2018; Hargrove et al., forthcoming) to chlorothalonil (Bravo 720 formulation) was used to compare directly with C_{max} values while the BMDL was multiplied by the in vitro exposure time (24 h) to create a C × T equivalent to the AUC values (Figure 9). Both the C_{max} and AUC retained dose metrics were remarkably consistent in corresponding tissues (larynx and trachea) between the nasal and oral models. For this particular example using the LOAEL exposure concentration from the 2-week rat inhalation study, both dose metrics were generally 2-fold or more below their corresponding in vitro dose metric (BMDL or BMDL C × T) depending upon aerosol size.

DISCUSSION

Comparisons of CFPD Predictions With Previous Models and Experimental Data

Although an extensive database exists for particle deposition and clearance in upper airways and lungs of animals and humans (see summaries by Lippman et al., 1980; Lippman and Schlesinger, 1984; Stuart, 1984; Asgharian et al., 2001; ICRP, 1994; Paquet et al., 2015), much of the available data were not reported for the specific sub-airway regions incorporated in the current CFPD models. The current CFPD-based simulations were thus
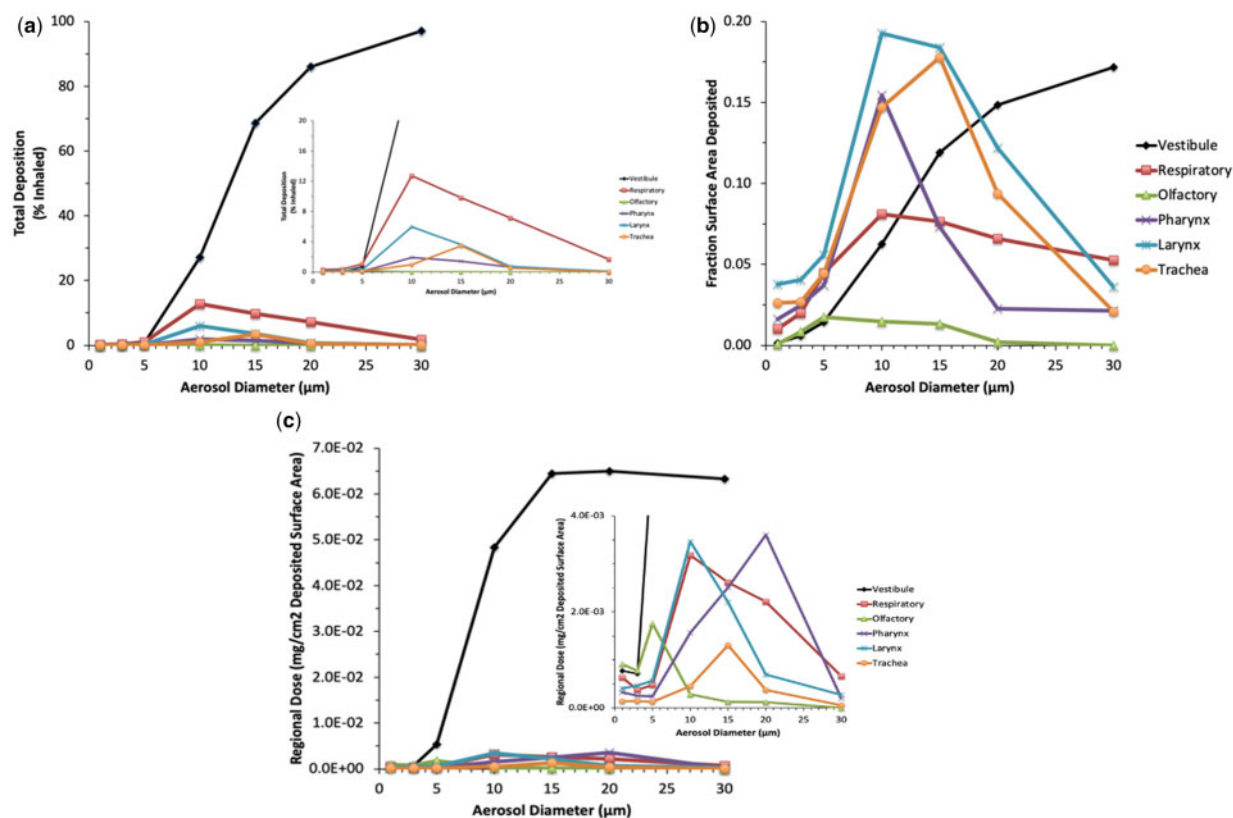
Figure 5. (A) Regional deposition (% inhaled), (B) fraction of regional surface areas with deposition, and (C) regional dose (mg/cm^2 deposited surface area) in the human nasal model following exposures to 1 mg/l aerosols with 1, 3, 5, 10, 15, 20, and 30 μm MMAD.

compared with other computational models developed from this experimental database including the widely used and extensively validated multiple path particle deposition model, MPPD (Anjilvel and Asgharian, 1995; Asgharian et al., 2001) and previous CFPD models as well as the limited experimental data that focused upon localized regions in upper airways of rats or humans.

Although the MPPD model focuses on the lung, it includes the upper respiratory tract (head) as an empirical filter for atmospheric aerosol exposures with an assumed aerosol size-dependent inhalability fraction based upon the analysis of Menache et al. (1995). Although not a perfect anatomic or physiological (ventilation profile) comparison with the current individualized CFPD models, MPPD simulations of deposition in the head region at the same species, ventilation rate, and exposure condition were compared with the current CFPD results at selected aerosol diameters.

For the rat, the total deposition of 2.72 μm monodisperse aerosols in the truncated CFPD model (upper conducting airways from the nostril to the upper trachea ending just below the larynx) was 58.55% of inhaled with the majority deposited in the nasal vestibule (53.1%) (Table 3). By comparison, MPPD predicted 69% of inhaled 2.72 μm monodisperse particles deposited in the head region assuming all particles were inhalable. This assumption (fully inhalable particles) is the closest to the conditions utilized in the CFPD model where particles were released into the airstream at the inlet to each nasal vestibule based upon airflow rates and aerosol concentration at each time step during the transient inhalation phase. Depending upon experimental techniques (eg a whole-body vs. a nose-only

exposure or use of a ventilator to drive inhalation), the inhalability fraction may deviate significantly below 1.0, leading to a wider range of potential inhalability-corrected deposition fractions predicted in the head versus the chest (trachea-bronchial and pulmonary airways).

Two experimental data sets (Kelly et al., 2001; Kuehl et al., 2012) also suggest that deposition of particles similar in size to the 2.72 μm MMAD aerosols from the chlorothalonil rat inhalation study can range from 10% to 50% of inhaled particles in the nasal region, depending upon the exposure techniques, aerosol characteristics (monodisperse vs. polydisperse, particle density), and analytical methods. Thus, the simulation results from the current CFPD model for the rat upper airways are comparable to the MPPD simulations and experimental data. For other aerosol materials that continue to rely upon in vivo rat versus human comparisons, additional simulations that account for polydisperse aerosol exposures encountered in rat bioassays may be necessary. Because this study highlights an alternative approach using CFPD-based tools for in vitro-in vivo comparisons with human cells, these additional rat simulations were not included even though the GSD's observed in the 2-week inhalation study indicated aerosol exposures were polydisperse.

For the human nasal model, total amounts deposited in the truncated model (upper conducting airways from the nostril to the upper trachea ending just below the larynx) at aerosol sizes of 1, 5, 10, and 30 μm were 0.56%, 2.35%, 48.8%, and 98.9% of inhaled aerosols, respectively (Tables 3 and 4). Corresponding MPPD predictions for the head region were 40.6%, 71.5%, 87.4%, and 99.8% of inhaled aerosol, respectively. Similar differences were observed in upper airways (mouth, pharynx, and larynx)

Table 5. Aerosol Deposition (% Inhaled and Total Deposited Dose Over Deposited Surface Area) for Each Annotated Region of the **Human Oral Breathing Model** Following Single Breath Exposure to 1 mg/l Aerosol at Sizes Ranging From 1 to 50 μm MMAD

Aerosol Diameter (μm)	Total Deposition (% Inhaled)	Regional Aerosol Deposition (% Inhaled)						Regional Aerosol Deposition (Total mg/cm² Deposited Surface Area)					
		Mouth (Lips + Oral Cavity)	Pharynx	Larynx	Trachea	Carina	Bronchi	Mouth (Lips + Oral Cavity)	Pharynx	Larynx	Trachea	Carina	Bronchi
1	1.3	0.3	0.03	0.1	0.055	0.02	0.8	1.86E-04	2.68E-05	7.01E-05	2.44E-05	2.33E-05	1.12E-04
3	2.0	0.6	0.07	0.2	0.079	0.03	1.0	1.54E-04	2.81E-05	8.13E-05	2.72E-05	2.19E-05	9.69E-05
5	4.7	1.5	0.16	0.3	0.151	0.06	2.5	2.11E-04	4.94E-05	1.34E-04	4.12E-05	2.68E-05	1.63E-04
10	31.0	7.2	0.82	4.7	1.196	0.37	16.7	7.51E-04	2.07E-04	1.50E-03	2.20E-04	1.22E-04	8.06E-04
15	69.1	22.9	7.88	12.4	5.457	1.52	18.9	2.24E-03	1.81E-03	3.82E-03	8.59E-04	4.79E-04	8.75E-04
20	87.8	53.9	16.15	7.9	3.798	0.71	5.3	4.59E-03	2.81E-03	2.33E-03	6.06E-04	2.40E-04	2.94E-04
30	96.8	84.2	8.85	2.0	0.919	0.33	0.4	7.33E-03	1.82E-03	6.04E-04	2.10E-04	2.06E-04	9.86E-05
50	99.5	97.0	2.28	0.3	0.004	0.0	0.0	1.43E-02	1.19E-03	1.85E-04	1.01E-05	0	0

Regional surface areas, fractional deposited surface areas are summarized in Supplementary S 7. Simulation results were truncated to a level of precision for calculation and display purposes and not to imply the level of certainty to the results.

for oral breathing simulations. For the human oral model, total amounts deposited were 0.5%, 2.0%, 12.7%, 43.1%, 78.0%, and 95.5% of inhaled at aerosol sizes of 1, 5, 10, 15, 20, and 30 μm, respectively. Corresponding MPPD predictions for the head region were 0.7%, 9.2%, 41.0%, 68.0%, 83.0%, and 94% inhaled, respectively. Thus, there is a difference in the breakpoints for the aerosol size-dependent increase in the deposition in the upper airways between the CFPD and MPPD predictions where CFPD models predict lower deposition of aerosols ≤15 μm in the extra-thoracic region. This difference is largely attributed to airway geometry differences between the imaging-based 3D CFPD from a single human and the generalized/averaged 1D MPPD model for the head region.

In an experimental study using human nasal molds derived from magnetic resonance imaging, Kelly et al. (2005) measured aerosol deposition for various sizes of monodisperse aerosols introduced at various continuous flowrates. In that study, deposition efficiencies in the nose ranged from <1% to 8% for particle sizes of 1–3 μm at 20 l/min continuous flow rates, then 10%–40% at 5 μm, and 80%–>95% for 8–10 μm particles. A CFPD model for one of the nasal molds and exposure conditions predicted similar deposition amounts of approximately 10%, 10%, and 90% for 1, 5, and 10 μm, respectively (Shanley et al., 2008). The current CFPD simulations compared reasonably well given the anatomic and airflow profile differences between these studies.

Another CFPD model that explored human variability in 4 ethnicities (4 subjects/ethnicity) in nasal extraction of aerosols and predicted wide ranges of deposition efficiencies in the nose (from <5% to >95% inhaled) for particles ranging from 5 to 20 μm with nearly complete deposition at 30 μm in all individuals (Keeler et al., 2015). This further indicates that critical factors in comparing CFPD or MPPD model outputs and experimental data are the individual's 3D anatomy, breathing rates used in the models versus experiments, and experimental conditions that affect inhalability (Menache et al., 1995).

Cross-Species Comparisons
Simulations of chlorothalonil-containing aerosol deposition in each region of the upper conducting airways of the rat and human were conducted to relate deposited doses of chlorothalonil across species under the same exposure condition at the MMAD used in the 2-week rat inhalation study (Bain, 2013). As expected, nasal scrubbing of aerosols in humans was far less significant than in rats. In this study, deposition in the rat nose accounted for over 58% of the inhaled, 2.72 μm diameter aerosols, whereas <1% of such aerosols were retained by the human nose under the same exposure condition. However, the human nose serves as an effective filter when aerosol diameters are ≥10 μm under normal breathing conditions. Regardless, the same general regions that showed the greatest susceptibility to chlorothalonil-induced cytotoxicity/contact irritation (anterior nose and larynx, and to a lesser degree the trachea and lung) were also the regions where higher local doses (mg CTN/cm² deposited surface) in both the nasal and oral human models (nose/mouth, pharynx and larynx, and to a lesser degree the trachea and bronchi) depending upon the aerosol sizes. Thus, when a particulate clearance model is developed for the rat that encompasses the upper airways similar to the Paquet et al. (2015) human model, a traditional comparison of retained doses across species could be developed. This was considered to be beyond the scope of this study because our focus is on a new approach method that utilizes human *in vitro* data as potential POD *in lieu* of additional animal studies.
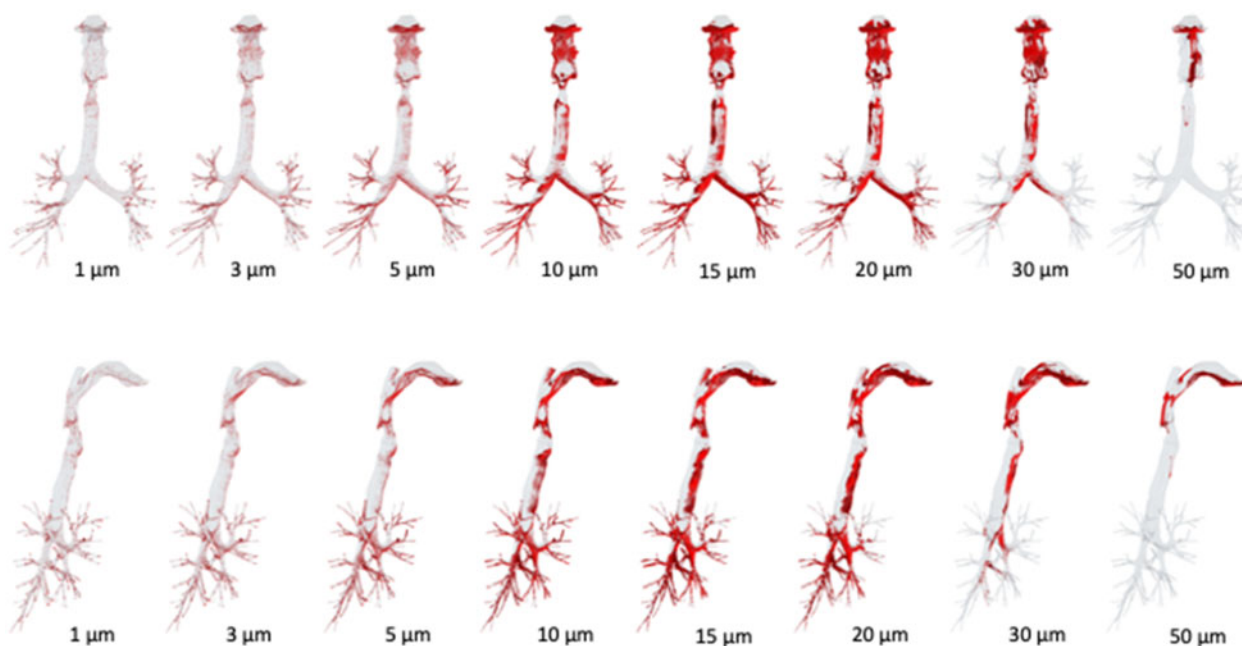
Figure 6. Deposition patterns in the human oral model following exposures to 1 mg/l aerosols with 1, 3, 5, 10, 15, 20, 30, and 50 μm MMAD aerosols. Top-front view; bottom-side view.

In Vivo/In Vitro Comparisons

As an alternate approach to traditional cross-species extrapolations, results from the CFPD/Clearance model-based dosimetry for humans exposed at the LOAEL air concentration (0.0011 mg CTN/l air) for the cytotoxicity observed in the 2-week rat study were compared with the BMDL for cytotoxicity determined from the *in vitro* study in human cells grown at the ALI (Vinall, 2017; Li *et al.*, 2018; Hargrove *et al.*, forthcoming). The authors used the MucilAir system (Epithelix Sàrl, Geneva, Switzerland) composed of basal stem cells, mucus-producing goblet cells, and ciliated cells isolated from the nasal region from 5 individual donors as a surrogate for bronchial epithelium as it was easier to obtain enough samples at the time the study was conducted. The overall BMDL for cytotoxicity was assessed by measuring transepithelial electrical resistance, lactate dehydrogenase release, and resazurin metabolism across a wide range of doses for each individual donor. Although using nasal epithelium may be considered a limitation for comparing responses in lower airways, for a direct acting, contact irritant/cytotoxicant like chlorothalonil that is affects all portal of entry or mucus membrane tissues, it is reasonable to assume that similar responses would be observed in cells isolated from nasal, tracheal, or bronchial regions of the respiratory airways. For other chemicals with different modes of action, this assumption may not be valid.

For this particular example, both C_{max} and AUC for retained local dose metrics were generally 2-fold or more below their corresponding *in vitro* dose metric (BMDL or BMDL C × T) depending upon aerosol size. The next highest chlorothalonil air concentration in the rat study was nearly 3-fold higher; thus, when the *in vitro* BMDL derived from human cells are compared with these specific human exposures and simulations of retained doses, the results fall within the range of the 2 lowest exposure concentrations that generally produced minimal to mild toxicity in the rat inhalation study (Supplementary Table 2). Although the current *in vivo/in vitro* comparison was only an example, HECs can now be derived for the *in vitro* BMDL's as a POD in assessing potential inhalation risks.

For realistic exposure scenarios for operators and residents, the inhalable exposures would likely consist of a distribution of aerosol particle sizes (polydisperse). Different aerosol concentrations of an active ingredient or polydisperse aerosol exposures could be estimated from the current simulations of monodisperse aerosol sizes using the current assumption of no aerosol-aerosol interactions as experimentally verified by Rosati *et al.* (2003) for stable, well-characterized aerosols. Work is ongoing to derive the HEC values for operator and residential risk assessment by integrating the results from this study, the *in vitro* study, as well as the inhalable particle size characterizations for chlorothalonil formulation use such as those by Flack *et al.* (2019).

Model Limitations and Future Directions

For both rats and humans, CFPD-based regional dose predictions for chlorothalonil represent only the initial deposited doses of chlorothalonil for each inhalation exposure. To translate deposited doses to species-specific local doses over multiple breaths and for repeated exposures required the use of a clearance model, such as the abbreviated Paquet *et al.* (2015) model used in this study. For direct-acting contact respiratory cytotoxicants like chlorothalonil, this may be considered an optimal *in silico* approach. For other types of aerosols that have volatile components, are highly soluble in mucus and tissues, or require tissue uptake or metabolism to produce toxicity to respiratory as well as systemic tissues, additional model complexity would be necessary (cf. Asgharian *et al.*, 2018; Corley *et al.*, 2012, 2015, Haghnegahdar *et al.*, 2018; Schroeter *et al.*, 2006, 2008, 2014).

More importantly for chlorothalonil, future *in silico* studies could include different ventilation profiles recommended for the rat (eg, EPA, 1994 vs. Alexander *et al.*, 2008 and Miller *et al.*, 2014), alternative breathing rates for humans, or additional human models to address more real-world exposure scenarios and variability in deposited dose predictions that may be important for certain risk assessments. Choice of dose metric
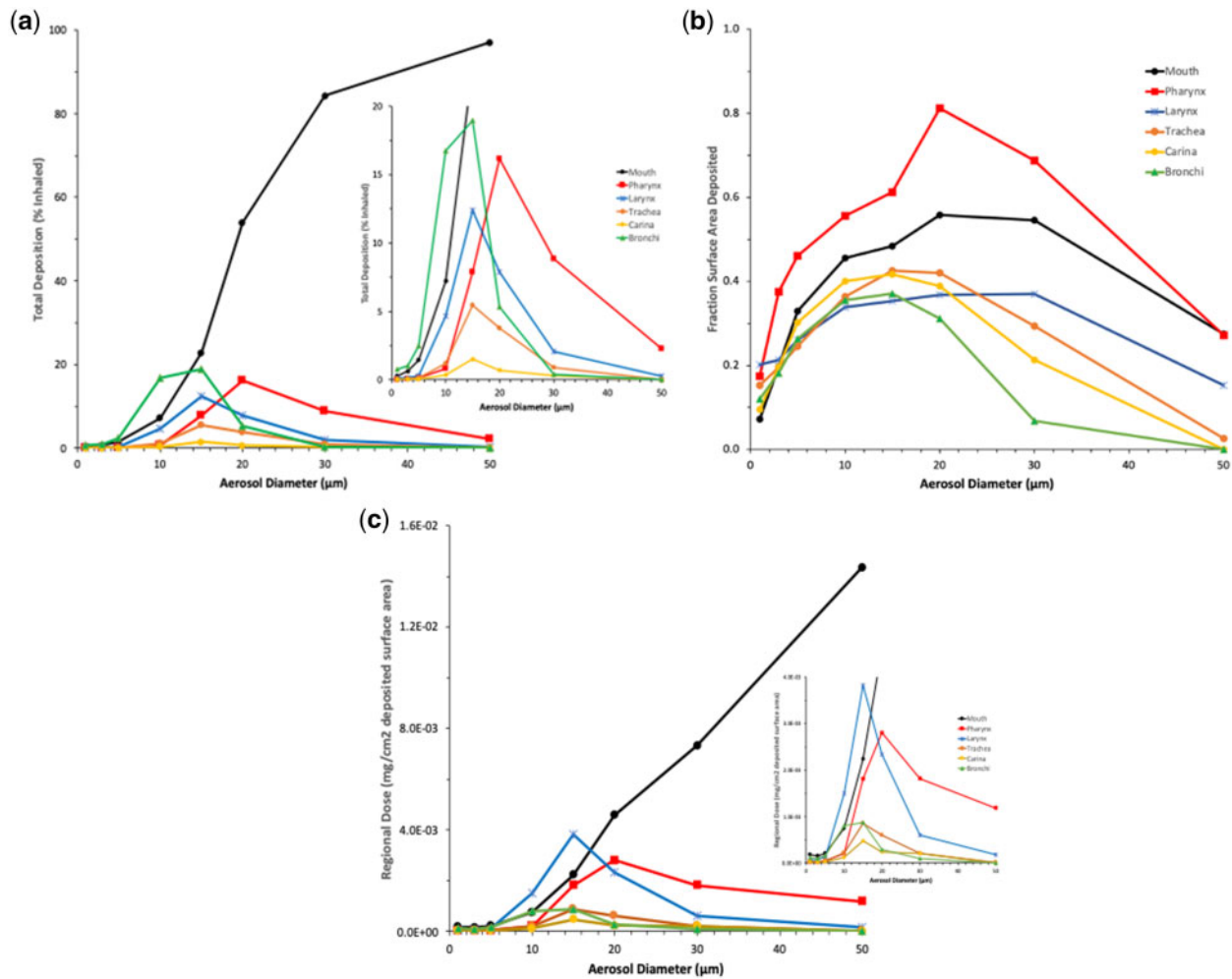
Figure 7. (A) Regional deposition (% inhaled), (B) fraction of regional surface areas with deposition, and (C) regional dose (mg/cm^2 deposited surface area) in the human oral model following exposures to 1 mg/l aerosols with 1, 3, 5, 10, 15, 20, 30, and 50 μm MMAD.

may also be refined by developing comparative 2D maps of lesion severity from animal studies with each potential dose metric to evaluate their relative strengths of correlation. Hygroscopic growth or aerosol-aerosol and aerosol-airflow interactions, which become increasingly important for larger aerosols or exposure concentrations, could also be evaluated to identify exposure conditions where such additional computational costs, which can be extensive, are necessary. To date, only a few such comparative CFD simulation studies have ever been published for complicated airways found in the respiratory systems of animals and humans as each model and simulation has historically taken considerable experimental and computational resources to develop and perform (cf. Calmet et al., 2018; Feng et al., 2016; Garcia et al., 2009; Keeler et al., 2015; Martonen and Wilson, 1983; Schroeter et al., 2016; Se et al., 2010). Fortunately, the time and effort to develop multiple models and perform the computational chemistry and physics processes associated with aerosols in even these complex, transient simulations continue to be reduced as technological advancements are made (Corley et al., 2015; Clark et al., 2017).

Lastly, if real-world exposures are found to occur that would lead to deposition in the deep lung beyond the regions included in current imaging-based CFPD models (typical 5–10 generations in

the human lung), alternative approaches for more efficient calculations of dose in this region may need to be adapted or developed. For these situations, CFPD models may be used to describe local doses in the upper conducting airways while lower-dimensional models, such as MPPD, may be used to focus on the lung. Alternatively, new hybrid multiscale approaches are currently being developed to extend CFPD models by including lower-dimensional models as boundary conditions for 3D CFPD models. These currently include 1D volume-filling airway skeletons, stochastic individual path models, idealized whole-lung airway models, and bidirectional coupling of individualized MPPD models with CFPD models that allow for estimations of aerosol transport and deposition throughout the respiratory system over the complete breathing cycle (Yin et al., 2010, 2013; Longest et al., 2012, 2016; Kolanjiyil and Kleinstreuer, 2016, 2017; Kuprat et al. 2016, 2019, 2021). As these new modeling tools become available, new insights into more complex exposure scenarios and individualized predictions of aerosol dosimetry that factor in a person's anatomy, physiology, and influences of a disease or dysfunction will be possible.

CONCLUSIONS

Aerosol droplet and associated chlorothalonil regional and site-specific deposition profiles were generated for the conducting
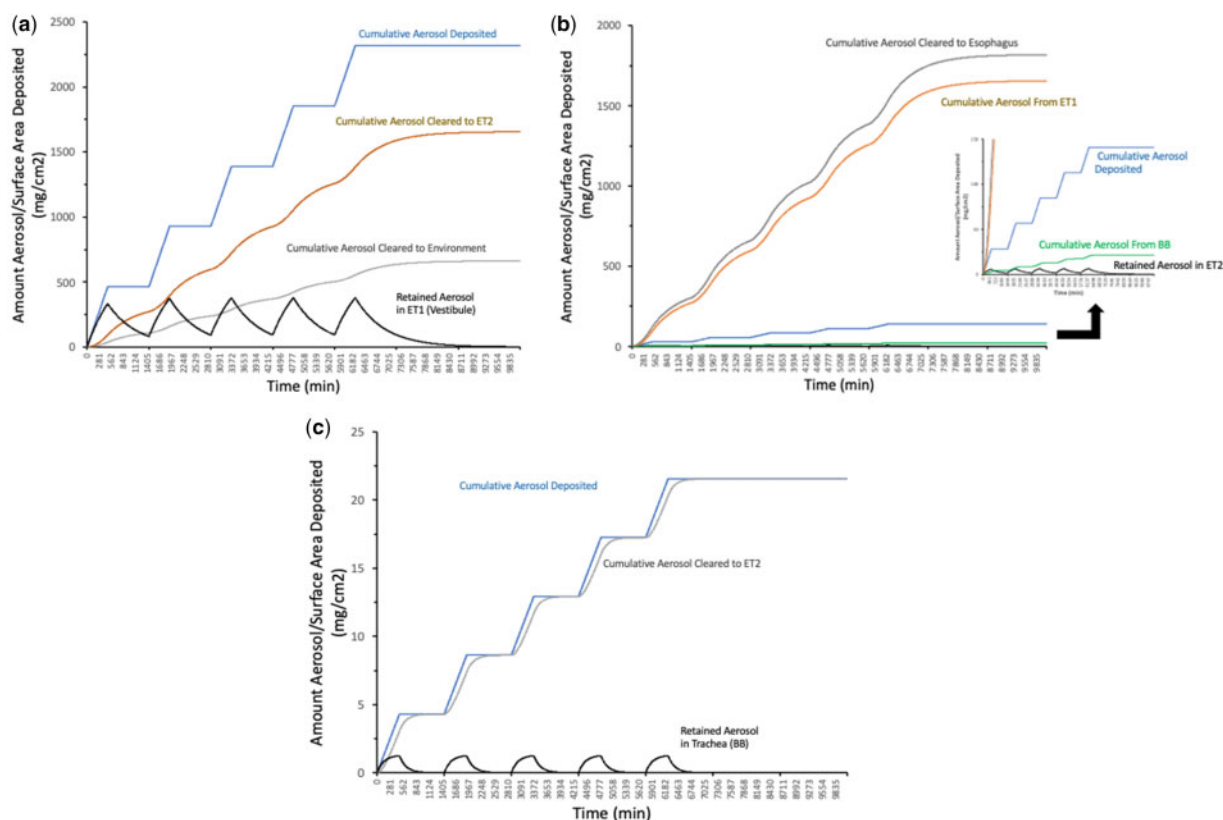
Figure 8. Total cumulative deposited, cleared, and retained doses of aerosol (mg) normalized to surface area deposited (cm²) of a representative 10 μm-sized aerosol in (A) nasal respiratory (ET1), (B) larynx (ET2), and (C) trachea (BB) regions for a nasal-breathing human exposed to 1 mg/l of aerosol for 8-h/day over 5 consecutive days.

airways of the rat and human (nose through the trachea for nasal breathing and mouth through bronchi for oral breathing) using CFD airflow/Lagrangian aerosol tracking models (CFPD). Significant species differences in airway deposition were predicted when humans and rats were exposed to the same aerosol size (2.72 μm) and concentration (4.03 mg aerosol/l air) used in the previous 2-week inhalation study with Bravo Weather Stik 720 SC formulation (Bain, 2013). For the rat, the size and complexity of nasal airway geometry resulted in >58% of inhaled aerosols deposited in the nose versus <1% of in the human nose. However, even though significantly less deposited in the human at the same exposure, the nasal respiratory epithelium, larynx, and trachea received the highest proportion of deposited dose, similar to locations in the rat where toxicity occurs. Given the site specificity demonstrated using anatomically and physiologically correct CFPD models, more accurate assessments of exposure-deposited dose-response relationships are now possible by comparing local deposited doses against site-specific lesions observed in rats; a process that is not feasible with lower-dimensional or compartmental models such as RDD and MPPD.

For formulations that typically produce aerosols ≥10 μm MMAD, the majority of human respiratory tissue exposures are in the anterior nasal cavity, especially the vestibule during nose breathing, which alone accounts for 27%, 69%, 86%, and 97% of total deposition of inhalable aerosols at 10, 15, 20, and 30 μm aerodynamic diameters, respectively under resting or light exercise conditions. For oral breathing, greater penetration of larger aerosols into the larynx, trachea, or bronchi occurs although there is a corresponding increase in the deposited surface area

versus nasal breathing. Thus, RDDs (mg/cm² deposited surface) are comparable between nasal and oral breathing. Resulting surface concentrations of active ingredients (formulation-specific) at these aerosol sizes can also vary widely, ranging from large surface areas receiving no exposure to several μg/cm² in areas of greatest deposition in the nose or mouth, larynx, and pharynx and bronchi, with very little aerosol penetration to the deep lung for either breathing modality.

By including a clearance model with the CFPD simulations of local airway deposition of a broad range of aerosol sizes during a single inhaled breath, various metrics of retained surface doses of the active ingredient such as the C_{max} or AUC for multiple days of 8-h/day exposures were used to compare potential human exposures to applied doses from *in vitro* studies with primary human respiratory epithelial cells grown in 3D cultures at the ALI. Both methods provide support for mode of action assessments, potential POD for BMD modeling of the response, calculations of HECs, and adjustments to default uncertainty factors for establishing exposure standards. By incorporating the physical/chemical properties of the formulation (eg, aerosol size, shape, density, percent active ingredient), the resulting CFD model predictions of airway deposition are also transferable to multiple pesticide compositions or active ingredients under the current breathing conditions. In the end, as more effort is applied to developing and validating new approaches to the assessment of inhalation toxicology, such as those described in this manuscript for other contact cytotoxicant/irritants like chlorothalonil, a corresponding reduction in animal studies could be achievable in the future.
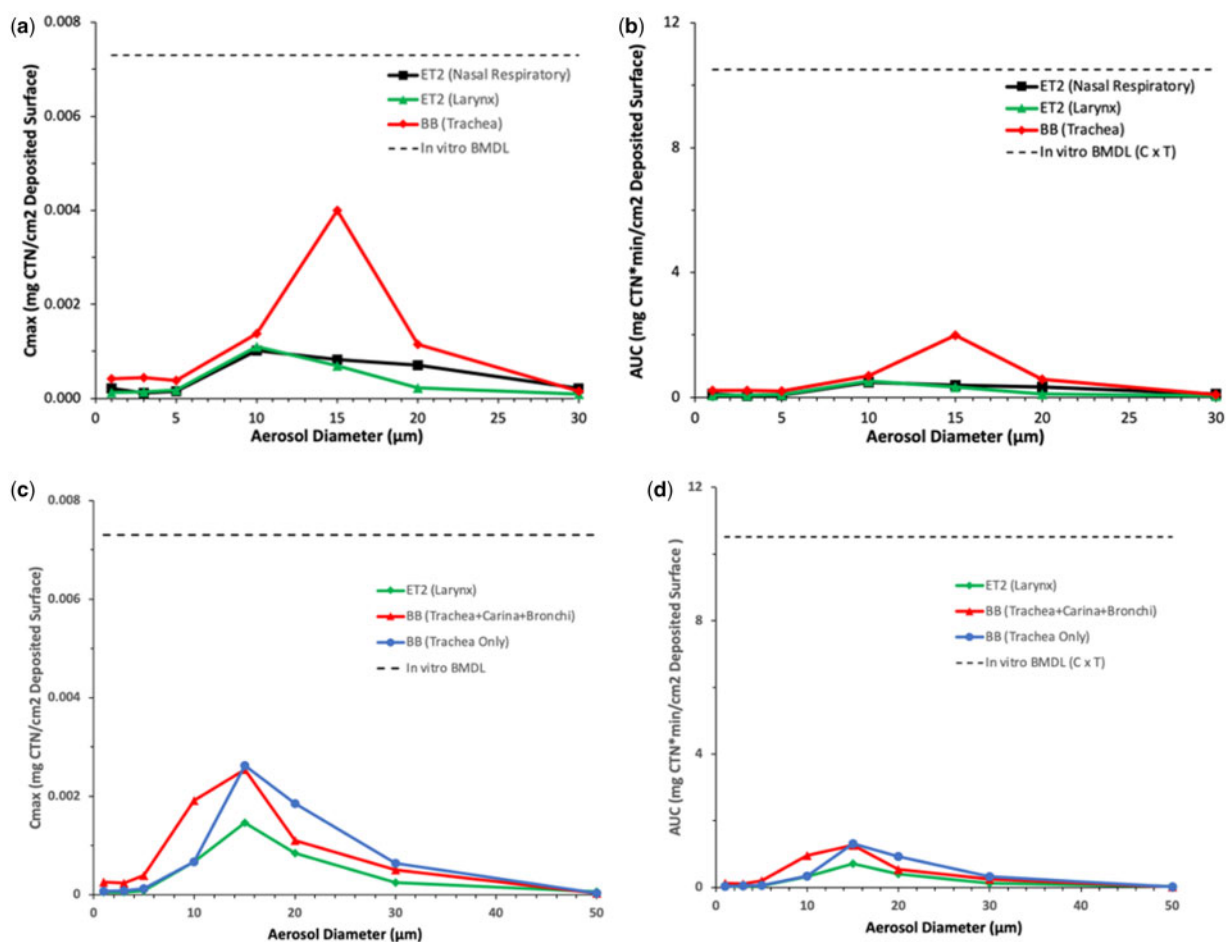
Figure 9. (A and C) Maximum retained doses (C_{max}; mg CTN/cm^2-deposited surface area) and (B and D) areas under the curve (AUC; mg CTN * min/cm^2-deposited surface area) in selected regions of a human exposed to the LOAEL aerosol concentration of chlorothalonil (CTN) from the Bain (2013) 2-week inhalation study (0.0011 mg/l) for 8-h/day over 5 consecutive days. Aerosol sizes ranged from 1 to 30 μm (nasal breathing model) or 50 μm (oral breathing model) MMAD. C_{max} and AUC values were determined for the final day of exposure followed by 2 days of no exposure.

SUPPLEMENTARY DATA

Supplementary data are available at *Toxicological Sciences* online.

Declarations of Conflicting Interests

The authors (P.M.H.) are former or current (T.S.R.) employees of Syngenta Crop Protection, LLC that produces chlorothalonil and funded the CFPD simulations and subsequent analyses. Author R.A.C. served as a consultant to Syngenta after retirement from PNNL to complete the project and manuscript preparation. The remaining authors (A.P.K., S.R.S., S.K., and K.Y.) declared no potential conflicts of interest with respect to the research, authorship, and/or publication of this article.

REFERENCES

Alexander, D. J., Collins, C. J., Coombs, D. W., Gilkison, I. S., Hardy, C. J., Healey, G., Karantabias, G., Johnson, N., Karlsson, A., Kilgour, J. D., *et al.* (2008). Association of inhalation toxicologists (AIT) working party recommendations for standard delivered dose calculation and expression in non-clinical aerosol inhalation toxicology studies with pharmaceuticals. *Inhal. Toxicol.* **20**, 1179–1189.

Anjilvel, S., and Asgharian, B. (1995). A multiple-path model of particle deposition in the rat lung. *Fund. Appl. Toxicol.* **28**, 41–50.

Asgharian, B., Hofmann, W., and Bergmann, R. (2001). Particle deposition in a multiple-path model of the human lung. *Aerosol. Sci. Technol.* **34**, 332–339.

Asgharian, B., Price, O. T., Rostami, A. A., and Pithawalla, Y. B. (2018). Deposition of inhaled electronic cigarette aerosol in the human oral cavity. *J. Aerosol Sci.* **116**, 34–47.

Bain, J. (2013). Chlorothalonil – (Bravo Weather Stik 720 SC) (A122531B) – 2-week inhalation toxicity study in rats with up to 14 days recovery. R&D Report of Syngenta Crop Protection, LLC. Project TK0177757.

Calmet, H., Kleinstreuer, C., Houzeaux, G., Kolanjiyil, A. V., Lehmkuhl, O., Olivares, E., and Vázquez, M. (2018). Subject-variability effects on micron particle deposition in human nasal cavities. *J. Aerosol Med.* **115**, 12–28.

Clark, A. R., Kumar, H., and Burrowes, K. S. (2017). Capturing complexity in lung system modeling. *Proc. Inst. Mech. Eng. Part H* **231**, 355–368.

Corley, R. A., Kabilan, S., Kuprat, A. P., Carson, J. P., Jacob, R. E., Minard, K. R., Teeguarden, J. G., Timchalk, C., Pipavath, S., Glenny, R., *et al.* (2015). Comparative risks of aldehyde constituents in cigarette smoke using transient computational fluid dynamics/physiologically based pharmacokinetic models of the rat and human respiratory tracts. *Toxicol. Sci.* **146**, 65–88.

Corley, R. A., Kabilan, S., Kuprat, A. P., Carson, J. P., Minard, K. R., Jacob, R. E., Timchalk, C., Glenny, R., Pipavath, S., Cox, T., *et al.* (2012). Comparative computational modeling of airflows and vapor dosimetry in the respiratory tracts of rat, monkey, and human. *Toxicol. Sci.* **128**, 500–516.

EPA (U.S. Environmental Protection Agency). 1994. Methods for derivation of inhalation reference concentrations and application of inhalation dosimetry. EPA 600/8-90/066F. October, 1994.

EPA (U.S. Environmental Protection Agency). 2016. *Process for Evaluating & Implementing Alternative Approaches to Traditional In Vivo Acute Toxicity Studies for FIFRA Regulatory Use.* Office of Pesticide Programs, Washington, DC. February 4, 2016.

EPA (U.S. Environmental Protection Agency). 2018. Strategic plan to promote the development and implementation of alternative test methods within the TSCA program. EPA-740-R1-8004. June 22, 2018.

EPA (U.S. Environmental Protection Agency). 2019. Peer review on evaluation of a proposed approach to refine the inhalation risk assessment for a point of contact toxicity: a case study using a new approach methodology (NAM). FIFRA Scientific Advisory Panel Meeting Minutes and Final Report No. 2019-01. April, 2019.

Feng, Y., Xu, Z., and Haghnegahdar, A. (2016). Computational fluid-particle dynamics modelling for unconventional inhaled aerosols in human respiratory systems. In *Aerosols – Science and Case Studies* (K. Volkov, Ed.), pp. 49–84. InTech Open Science, Rijeka, Croatia.

Flack, S. L., Ledson, T. M., and Ramanarayanan, T. S. (2019). Particle size characterization of agricultural sprays collected on personal air monitoring samplers. *J. Agric. Safety Health* **25**, 91–103.

Garcia, G. J. M., Schroeter, J. D., Segal, R. A., Stanek, J., Foureman, G. L., and Kimbell, J. S. (2009). Dosimetry of nasal uptake of water-soluble and reactive gases: a first study of interhuman variability. *Inhal. Toxicol* **21**, 607–618.

Haghnegahdar, A., Feng, Y., Chen, X., and Lin, J. (2018). Computational analysis of deposition and translocation of inhaled nicotine and acrolein in the human body with e-cigarette puffing topographies. *Aerosol Sci. Technol* **52**, 483–493.

Hargrove, M. M., Parr-Dobrzanski, B., Li, L., Contant., S., Wallace, J., Hinderliter, P. M., Wolf. D. C., and Charlton, A. (2021). Use of the Mucilair Airway Assay, a New Approach Methodology, for Evaluating the Safety and Inhalation Risk of Agrochemicals. Appl. In Vitro Toxicol. Forthcoming.

IARC (International Agency for Research on Cancer); World Health Organization. (1999). Some chemicals that cause tumors of the kidney or urinary bladder in rodents and some other substances. In *IARC Monographs on the Evaluation of Carcinogenic Risks to Humans*, Vol. **73**, pp. 183–193. IARCPress, Lyons, France.

ICRP (International Commission on Radiological Protection). (1994). *Human Respiratory Tract Model for Radiological Protection.* ICRP Publication 66. Ann. ICRP 24(1-3). Pergamon Press, Oxford, UK.

Kabilan, S., Suffield, S. R., Recknagle, K. P., Jacob, R. E., Einstein, D. R., Kuprat, A. P., Carson, J. P., Colby, S. M., Saunders, J. H., Hines, S. A., *et al.* (2016). Computational fluid dynamics modeling of *Bacillus anthracis* spore deposition in rabbit and human respiratory airways. *J. Aerosol Sci.* **99**, 64–77.

Keeler, J. A., Patki, A., Woodard, C. R., and Frank-Ito, D. O. (2015). A computational study of nasal spray deposition pattern in four ethnic groups. *J. Aerosol Med. Pulm. Drug Deliv.* **28**, 1–14.

Kelly, J. T., Bobbitt, C. M., and Asgharian, B. (2001). In vivo measurement of fine and coarse aerosol deposition in the nasal airways of female Long-Evans rats. *Toxicol. Sci.* **64**, 253–258.

Kelly, J. T., Asgharian, B., and Wong, B. A. (2005). Inertial particle deposition in a monkey nasal mold compared with that in human replicas. *Inhal. Toxicol* **17**, 823–830.

Kimbell, J. S., Subramaniam, R. P., Gross, E. A., Schlosser, P. M., and Morgan, K. T. (2001). Dosimetry modelling of inhaled formaldehyde: comparisons of local flux predictions in the rat, monkey, and human nasal passages. *Toxicol. Sci.* **64**, 100–110.

Kolanjiyil, A., and Kleinstreuer, C. (2016). Computationally efficient analysis of particle transport and deposition in a human whole-lung airway model. Part 1: theory and model validation. *Comput. Biol. Med* **79**, 193–204.

Kolanjiyil, A., and Kleinstreuer, C. (2017). Computational analysis of aerosol-dynamics in a human whole-lung airway model. *J. Aerosol Sci.* **114**, 301–316.

Kuehl, P. J., Anderson, T. L., Candelaria, G., Gershman, B., Harlin, K., Hesterman, J. Y., Holmes, T., Hoppin, J., Lackas, C., Norenberg, P., *et al.* (2012). Regional particle size dependent deposition of inhaled aerosols in rats and mice. *Inhal. Toxicol.* **24**, 27–35.

Kuempel, E. D., Sweeney, L. M., Morris, J. B., and Jarabek, A. M. (2015). Advances in inhalation dosimetry models and methods for occupational risk assessment and exposure limit derivation. *J. Occup. Environ. Hyg.* **12**, S18–S40.

Kuprat, A. P., Kabilan, S., Price, O., Asgharian, B., and Corley, R. A. (2016). Multiscale modeling of aerosol deposition in the complete respiratory tracts of animals and humans. Abst. #2215. 55th Annual Meeting of the Society of Toxicology. New Orleans, LA. March 13–17, 2016.

Kuprat, A. P., Jalali, M., Jan, T., Corley, R. A., Asgharian, B., Price, O., Singh, R., Colby, S., Thomas, D., and Darquenne, C. (2019). Setting the stage for computationally efficient multiscale lung modeling of aerosol dosimetry. Abst. # AB-40. In *Third*

Aerosol Dosimetry Conference, Inhaled Aerosol Dosimetry: Models, Applications and Impact. Irvine, CA, Oct. 10–12, 2019.

Kuprat, A. P., Jalali, M., Jan, T., Corley, R. A., Asgharian, B., Price, O., Singh, R., Colby, S., and Darquenne, C. (2021). Efficient bi-directional coupling of 3D computational fluid-particle dynamics and 1D multiple path particle dosimetry lung models for multiscale modeling of aerosol dosimetry. *J. Aerosol Sci.* **151**, 105647.

Li, L., Mosquin, P., and Brambilla, D. (2018) Chlorothalonil - Benchmark dose (BMD) analysis of MucilAir data to establish a toxicological point of departure (POD) for use in human risk assessment. Unpublished Final Report: 0212613.015; MRID: 50610401. Syngenta Crop Protection, LLC, Greensboro, NC. (Publicly available at: EPA Docket FIFRA SAP Meeting Dec. 4–7, 2018, EPA-HQ-OPP-2018-0517. https://www.epa.gov/sap/meeting-materials-december-4-6-7-2018-scientific-advisory-panel-0.)

Lippman, M., and Schlesinger, R. B. (1984). Interspecies comparisons of particle deposition and mucociliary clearance in tracheobronchial airways. *J. Toxicol. Env. Health* **13**, 441–469.

Lippman, M., Yeates, D. B., and Albert, R. E. (1980). Deposition, retention, and clearance of inhaled particles. *Br. J. Ind. Med* **37**, 337–362.

Longest, P. W., Tian, G., Khajeh-Hosseini-Dalasm, N., and Hindle, M. (2016). Validating whole-airway CFD predictions of DPI aerosol deposition at multiple flow rates. *J. Aerosl Med. Pulm. Drug Deliv.* **29**, 461–481.

Longest, P. W., Tian, G., Walenga, R. L., and Hindle, M. (2012). Comparing MDI and DPI aerosol deposition using *in vitro* experiments and a new stochastic individual path (SIP) model of the conducting airways. *Pharm. Res* **29**, 1670–1688.

Martonen, T. B., and Wilson, A. F. (1983). The influence of hygroscopic growth upon the deposition of bronchodilator aerosols in upper human airways. *J. Aerosol Sci.* **14**, 208–211.

Menache, M. G., Miller, F. J., and Raabe, O. G. (1995). Particle inhalability curves for humans and small laboratory animals. *Ann. Occup. Hyg.* **39**, 317–328.

Miller, F. J., Asgharian, B., Schroeter, J. D., Price, O., Corley, R. A., Einstein, D. R., Jacob, R. E., Cox, T. C., Kabilan, S., and Bentley, T. (2014). Respiratory tract lung geometry and dosimetry model for male Sprague-Dawley rats. *Inhal. Toxicol.* **26**, 524–544.

Mozzachio, A. M., Rusiecki, J. A., Hoppin, J. A., Mahajan, R., Patel, R., Beane-Freeman, L., and Alavanja, M. C. R. (2008). Chlorothalonil exposure and cancer incidence among pesticide applicator participants in the agricultural health study. *Environ. Res.* **108**, 400–403.

NRC (National Research Council). 2007. *Toxicity Testing in the 21st Century: A Vision and a Strategy*. National Academy Press, Washington, DC.

Paquet, F., Etherington, G., Bailey, M. R., Leggett, R. W., Lipsztein, J., Bolch, W., Eckerman, K. F., Harrison, J. D., and ICRP (2015). ICRP Publication 130: Occupational Intakes of Radionuclides: Part 1. *Ann. ICRP.* **44**, 5–188.

Rosati, J. A., Leith, D., and Kim, C. S. (2003). Monodisperse and polydisperse aerosol deposition in a packed bed. *Aerosol Sci. Technol.* **37**, 528–535.

Schroeter, J. D., Asgharian, B., Price, O. T., Kimbell, J. S., Kromidas, L., and Singal, M. (2016). Simulation of the phase change and deposition of inhaled semi-volatile liquid droplets in the nasal passages of rats and humans. *J. Aerosol Sci.* **95**, 15–29.

Schroeter, J. D., Campbell, J., Kimbell, J. S., Conolly, R. B., Clewell, H. J., and Andersen, M. E. (2014). Effects of endogenous formaldehyde in nasal tissues on inhaled formaldehyde dosimetry predictions in the rat, monkey, and human nasal passages. *Toxicol. Sci.* **138**, 412–424.

Schroeter, J. D., Kimbell, J. S., Bonner, A. M., Roberts, K. C., Andersen, M. E., and Dorman, D. C. (2006). Incorporation of tissue reaction kinetics in a computational fluid dynamics model for nasal extraction of inhaled hydrogen sulphide in rats. *Toxicol. Sci.* **90**, 198–207.

Schroeter, J. D., Kimbell, J. S., Gross, E. A., Willson, G. A., Dorman, D. C., Tan, Y. M., and Clewell, H. J. (2008). Application of physiological computational fluid dynamics models to predict interspecies nasal dosimetry of inhaled acrolein. *Inhal. Toxicol.* **20**, 227–243.

Se, C. M. K., Inthavong, K., and Tu, J. (2010). Inhalability of micron particles through the nose and mouth. *Inhal. Toxicol.* **22**, 287–300.

Shanley, K. T., Zamankhan, P., Ahmadi, G., Hopke, P. K., and Cheng, Y. S. (2008). Numerical simulations investigating the regional and overall deposition efficiency of the human nasal cavity. *Inhal. Toxicol.* **20**, 1093–1100.

Stuart, B. O. (1984). Deposition and clearance of inhaled particles. *Env. Health Perspect.* **55**, 369–390.

Vinall, J. (2017). Chlorothalonil – In vitro measurement of the airway irritation potential of Bravo 720 SC formulation using MucilAirTM tissues from five different donors. Final Report Amendment 2 of Syngenta Limited, Bracknell, Berkshire, UK. (Publicly available at: EPA Docket FIFRA SAP Meeting Dec. 4–7, 2018, EPA-HQ-OPP-2018-0517. https://www.epa.gov/sap/meeting-materials-december-4-6-7-2018-scientific-advisory-panel-0.)

Wilkinson, C. F., and Killeen, J. C. (1996). A mechanistic interpretation of the oncogenicity of chlorothalonil in rodents and an assessment of human relevance. *Reg. Toxicol. Pharmacol.* **24**, 69–84.

Yin, Y., Choi, J., Hoffman, E. A., Tawhai, M. H., and Lin, C. L. (2010). Simulation of pulmonary air flow with a subject-specific boundary condition. *J. Biomech.* **43**, 2159–2163.

Yin, Y., Choi, J., Hoffman, E. A., Tawhai, M. H., and Lin, C. L. (2013). A multiscale MDCT image-based breathing lung model with time-varying regional ventilation. *J. Comp. Phys.* **244**, 168–192.